Geophysical identification of permafrost in Livingston Island, maritime Antarctica

Christian Hauck,[1,2] Gonçalo Vieira,[3] Stephan Gruber,[1,4] Juanjo Blanco,[5] and Miguel Ramos[5]

Received 2 May 2006; revised 5 February 2007; accepted 24 April 2007; published 21 June 2007.

[1] The current permafrost distribution on Livingston Island, South Shetland Islands, maritime Antarctic, was investigated using electrical resistivity tomography, refraction seismics, and shallow borehole temperatures. The field sites include different geological and geomorphological settings, including ice cored moraines and bedrock sites with debris covers of different thickness. Two-dimensional geophysical inversion schemes were used to analyze spatial heterogeneity at field sites and to detect isolated occurrences of ground ice. Results confirm that permafrost is widespread on Livingston Island, with high ice content in ice cored moraines and little in the cracks and fissures of frozen bedrock. Specific electrical resistivity values range from 10,000–40,000 ohm-m (frozen unconsolidated material) to 1500–10,000 ohm-m (frozen quartzite/shale). Combining seismic *P* wave velocities and specific electrical resistivities, a typical "roof-type" distribution was found with maximum resistivities coinciding with *P* wave velocities around 3000 m/s and decreasing resistivities for both increasing and decreasing velocities.

Citation: Hauck, C., G. Vieira, S. Gruber, J. Blanco, and M. Ramos (2007), Geophysical identification of permafrost in Livingston Island, maritime Antarctica, *J. Geophys. Res.*, *112*, F02S19, doi:10.1029/2006JF000544.

1. Introduction

[2] Permafrost is recognized by the World Climate Research Programme as a key element of the Earth System upon which future research efforts should focus [*Intergovernmental Panel on Climate Change*, 2001]. In contrast to numerous studies in the Arctic and mountainous areas, detailed studies on the characteristics of permafrost and its response to climate change are relatively few in the Antarctic [*Hall*, 2002]. The main reason is the very scarce network of permafrost monitoring boreholes in the region, as well as the small number of active layer monitoring sites. Such networks are important for validating and calibrating climate models and for understanding the dynamics of Antarctic permafrost in the framework of global change.

[3] Two core projects of the International Polar Year 2007–2008 where Antarctic permafrost plays a central role have recently been approved: Antarctic and Sub-Antarctic Permafrost, Soils and Periglacial Environments (ANTPAS) (Project 33) and Permafrost Observatory Project–Thermal State of Permafrost (TSP) (Project 50). As a precursor to future permafrost monitoring initiatives, the current permafrost distribution should be determined to establish a baseline for assessing an impact of climate change on permafrost in Antarctica. The research presented here is part of both initiatives and, being motivated by the evaluation and characterization of possible borehole locations in the South Shetland Islands, seeks to characterize permafrost and its distribution on Livingston Island/South Shetland Islands using geophysical techniques. Geophysical properties of permafrost occurrences are determined for facilitating permafrost assessment in future geophysical campaigns in the maritime Antarctic.

[4] Present and Quaternary periglacial processes and landforms in continental and maritime Antarctica have been increasingly studied in recent years (for a review, see *Bockheim and Hall* [2002] and *Hall* [2002]). In contrast to the Antarctic continent, the islands near the Antarctic Peninsula are more affected by eastward moving cyclonic depressions with high precipitation and less severe temperatures than on the continent. The South Shetland Islands are a mountainous and extensively glaciated group of islands, where occurrences of permafrost are restricted to bedrock and ice-free regions near the coast, but with reported thicknesses of up to 100 m [*Bockheim and Hall*, 2002]. The nature and horizontal and vertical extent of cryogenic processes varies greatly between the islands, such that simple comparisons and predictions for future evolution are difficult with present data sets [*Hall*, 2002].

[5] One possibility to improve knowledge of ground ice distribution at larger spatial scales is by extensive use of

[1]Glaciology and Geomorphodynamics Group, Geographical Institute, University of Zurich, Zurich, Switzerland.
[2]Institute for Meteorology and Climate Research, Forschungszentrum Karlsruhe, University of Karlsruhe, Karlsruhe, Germany.
[3]Centre for Geographical Studies, Faculdade de Letras, University of Lisbon, Lisbon, Portugal.
[4]Laboratoire Environnements, Dynamiques et Territoires de la Montagne, Centre Interdisciplinaire Scientifique de la Montagne, Université de Savoie, Savoie, France.
[5]Department of Physics, University of Alcalá, Alcalá de Henares, Spain.

0148-0227/07/2006JF000544

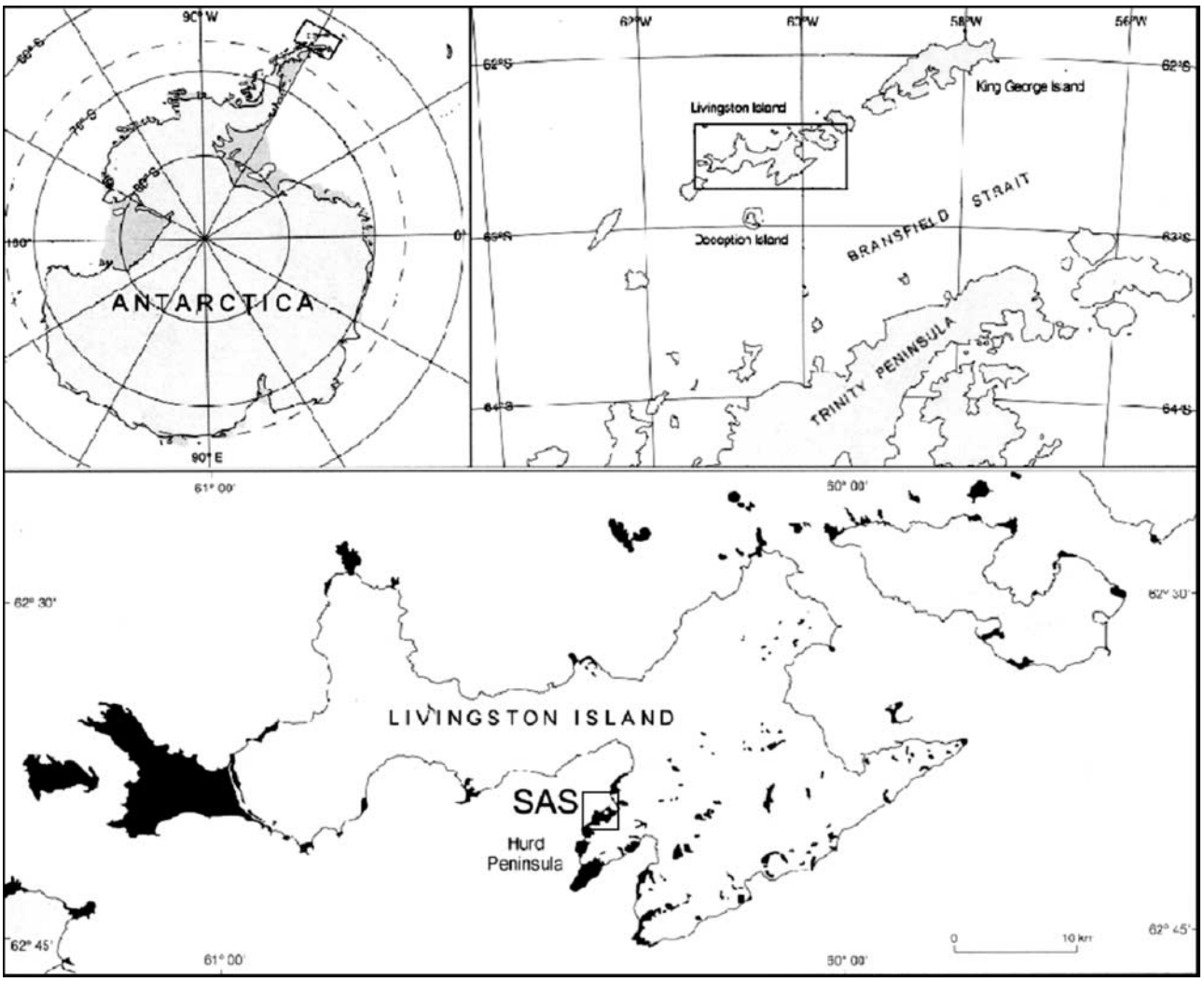

Figure 1. Map of the study area in the South Shetland Islands and field site locations on Livingston Island. Small rectangle in the bottom map shows location of detailed map in Figure 3.

geophysical techniques. Geophysical techniques are low-impact methods that are especially useful in such sensitive and protected areas as the Antarctic. Electromagnetic (airborne induction or radar techniques) and reflection seismic methods are commonly used to determine ice thickness of glaciers and ice caps [*Hubbard and Glasser*, 2005], whereas electric, electromagnetic and refraction seismic methods are the preferred choice on frozen ground [e.g., *McGinnis et al.*, 1973; *Fournier et al.*, 1990; *Guglielmin et al.*, 1997].

[6] Permafrost distribution in Livingston Island (Figure 1) has been studied using geomorphological evidence [e.g., *Serrano and López-Martínez*, 2000; *Vieira and Ramos*, 2003] and direct ground temperature monitoring in shallow boreholes [*Ramos et al.*, 2002; *Ramos and Vieira*, 2003]. Geomorphological observations by *Serrano and López-Martínez* [2000] and *Serrano* [2003] indicate that permafrost is widespread in the South Shetlands above 30 m above sea level (asl). Borehole temperatures show that permafrost is present in the Hurd Peninsula at 275 m asl at ca. 1 m depth, but the lower limit of permafrost has not yet been delineated [*Ramos and Vieira*, 2003].

[7] Geophysical studies on the distribution of permafrost in Livingston Island are few and have focused on the inner structure of the Hurd rock glacier [*Serrano et al.*, 2004]. One-dimensional vertical electrical soundings revealed a high-resistivity layer (10,000–150,000 ohm-m) at a depth of 0.4 to 3 m with a thickness of 2 m and was interpreted as ice-rich permafrost. Other electrical soundings conducted by *Bergamín et al.* [1997] were concerned with the basement morphology of the Caleta Española (Spanish Antarctic Station beach). This study is of significance for permafrost research because several sites were found to have a thin layer (0.5–1 m) at shallow depth (0.5–2 m) with high resistivities (35,000–77,000 ohm-m). This layer, interpreted as ice-rich permafrost, was found in the raised beach deposits near the slope to the southwest of the Spanish Antarctic Station at altitudes between 15 and 20 m asl. Results from *Serrano et al.* [2004] and *Bergamín et al.* [1997] demonstrate the presence of shallow, ice-rich permafrost bodies, both in the rock glacier and in the raised-beach cobble deposits and confirm the importance of geoelectrical surveys for characterizing permafrost in the maritime Antarctic. However, few surveys have been con-

Table 1. Geophysical Profiles Conducted on Livingston Island During the 2006 Spanish Antarctic Campaign

	Electrical Resistivity Tomography		Refraction Seismic Tomography		
Location	Length, m	Depth, m	Length, m	Depth, m	Characteristics[a]
Site A: Caleta Argentina	110	18	-	-	ice cored moraine
Site B: Caleta Española	28, 126	4, 20	22	5	ice cored moraine
Site C: Refugio de motos	30, 110	5, 18	-	-	bedrock
Site D: Incinerador	105	16	55	10	ash, bedrock, BH
Site E: Collado Ramos	2 × 150	22	55	8	bedrock
Site F: Reina Sofia Hill	30, 90	5, 15	22	5	Bedrock, BH

[a]BH is existence of a shallow borehole.

ducted with the objective of studying permafrost in different geological and geomorphological settings, and therefore not much information on permafrost distribution has been provided. In addition, the lack of two-dimensional information limits the assessment of permafrost distribution and characteristics to general and averaged findings.

2. Methods

[8] From the large number of possible geophysical methods two complementary techniques were chosen, in order to reduce the ambiguity of each single method and to enhance reliability. The applied methods were: electrical resistivity tomography (ERT) and refraction seismic tomography (RST). ERT and RST surveys were conducted in the study area during January 2006 as part of the Spanish Antarctic campaign (see Table 1). Temperatures in shallow boreholes were used for cross validating the resulting data sets.

2.1. Electrical Resistivity Tomography (ERT)

[9] Because a marked increase in electrical resistivity occurs at the freezing point, electrical methods are most suitable to detect, localize and characterize structures containing frozen material. This phenomenon has long been recognized in several field and laboratory studies [e.g., *Hoekstra et al.*, 1975] and electrical methods have therefore been applied in numerous permafrost studies (for a review, see *Scott et al.* [1990] and *Hauck and Vonder Mühll* [2003a]). On the basis of the number of scientific publications in the last decade and the large variety of applications, the tomographic variant of the method (electrical resistivity tomography, ERT) may be the most universally applicable method, although it should be used in combination with another geophysical method, if possible. Owing to the recent development of multielectrode resistivity systems and commercially available two-dimensional inversion schemes for data processing, this method is comparatively easy to apply, even in very heterogeneous mountain and remote terrain. As with most geophysical techniques the resistivity model obtained is not unambiguous and depends on data quality, measurement geometry, and the choice of inversion parameters [*Hauck and Vonder Mühll*, 2003b].

[10] Tomographic methods such as ERT overcome the limitations of one-dimensional methods as vertical electrical soundings (VES), which are based on the assumption of horizontally homogeneous subsurface conditions. Under heterogeneous ground conditions, interpretation of VES data can be difficult, as lateral variations along the survey line can influence results significantly and individual anomalies will not show explicitly in the results [*Kneisel et al.*, 2000]. ERT overcomes this problem by using two-dimensional data inversion schemes, which provide more accurate resistivity models of the subsurface [*Daily et al.*, 2004].

[11] ERT requires multiple resistivity measurements with varying electrode spacings along a profile line. Multielectrode systems are commonly used to acquire apparent resistivity data sets. If multielectrode instruments are unavailable, tomographic data sets can be obtained using a standard four-channel resistivity meter and multiple single apparent resistivity measurements with different electrode spacings and midpoints. Within this study ERT measurements were conducted using a four-channel Oyo McOhm resistivity meter with up to 33 electrodes and electrode spacings between 1 m and 5 m, depending on the desired investigation depth. The resistivity meter was subsequently connected to various electrode quadrupoles in Wenner configuration to yield an apparent resistivity data set suitable for tomographic inversion. Although this approach is more time consuming and requires more field personnel than multielectrode systems, it is a feasible measurement approach in cases where a multielectrode system is unavailable.

[12] The observed apparent resistivities were inverted using the tomographic inversion scheme Res2DINV [*Loke and Barker*, 1995]. Inversion parameters were chosen according to *Hauck and Vonder Mühll* [2003b] to obtain reliable results in cases of strong resistivity contrasts.

2.2. Refraction Seismic Tomography (RST)

[13] Refraction seismic investigations have a long tradition in permafrost studies [e.g., *Timur*, 1968; *Zimmerman and King*, 1986; *King et al.*, 1988]. A sharp increase of *P* wave velocity at the freezing point is used to differentiate between frozen and unfrozen material. *P* wave velocity and specific resistivity distribution can be used in complementary fashion to obtain information about the presence of frozen material. The method is especially useful for determining the location of top of the permafrost layer, as the contrast in *P* wave velocity between the overlying unfrozen layer (active layer, 400–1500 m/s) and the permafrost body (2000–4000 m/s) is typically large [*Hauck and Vonder Mühll*, 2003a]. Large ice bodies can usually be detected, because ice has a very distinct *P* wave velocity (around 3500–3750 m/s). The absence of permafrost in unconsolidated material can be inferred if sufficiently low *P* wave velocities (<1000 m/s) are observed. Differentiation between frozen and unfrozen bedrock with low ice content is difficult,

Table 2a. Mean Annual Air Temperatures in South Shetland Islands and Antarctic Peninsula Region for Different Periods and Stations[a]

Antarctic Station	Latitude	Longitude	Altitude, m asl	Period	MAAT, °C
Esperanza	63.4°S	57.0°W	13	1960–2006	−5.2
Faraday/Vernadsky	65.4°S	64.4°W	11	1947–2004	−3.9
Arctowski	62.1°S	59.0°W	-	1977–1996	−1.6
Ferraz	62.1°S	58.4°W	-	1986–2005	−1.8
Great Wall	62.2°S	59.0°W	10	1987–2006	−1.9
King Sejong	62.2°S	58.7°W	11	1988–2006	−1.8
Marsh	62.4°S	58.9°W	10	1987–2006	−2.3
Jubany	62.2°S	58.6°W	4	1987–2006	−1.6
Bellinghausen	62.2°S	58.9°W	16	1968–2006	−2.4
Deception	63.0°S	60.7°W	8	1959–1967	−3.2
Total of all stations					−2.6
Total without 1, 2, 10					−1.9

[a]Data are taken from http://www.antarctica.ac.uk/met/READER/surface/stationpt.html. MAAT is mean annual air temperatures.

as the range of *P* wave velocities can be quite similar [*Hauck et al.*, 2004].

[14] In permafrost studies, refraction seismic interpretation techniques are usually based on simple planar layer models, commonly restricted to two or three layers. This simplistic approach may be of limited use for very heterogeneous ground conditions. As with the ERT technique, tomographic inversion schemes can be used for reliable 2D interpretation [*Musil et al.*, 2002].

[15] A Geometrics seismograph with 12 channels and geophone spacing between 2 m and 5 m was used for seismic data acquisition. Shotpoints were generally located between adjacent geophones, using a sledgehammer as source. The comparatively small size of the data set allows for manual determination of first arrival times, which are inverted using the two-dimensional tomographic inversion approach introduced by *Lanz et al.* [1998].

2.3. Ground Temperature Measurements

[16] Shallow boreholes for ground temperature monitoring were installed in January 2000 at Incinerador (35 m asl) and Reina Sofia Hill (275 m asl) [*Ramos and Vieira*, 2003]. The Incinerador borehole is in quartzite and is 2.4 m deep. The Reina Sofia Hill borehole was drilled in a matrix-supported diamict to a depth of 1.1 m. The boreholes are sealed hermetically using a waterproof cylinder. Ground temperatures are monitored at hourly intervals at six (Incinerador) and four (Reina Sofia) different depths using NTC-10K thermistors and tiny tag miniature loggers (Gemini) with a precision of 0.1°C. Owing to technical problems the 6-year series is incomplete.

3. Study Area: Hurd Peninsula

3.1. General Characteristics

[17] Hurd Peninsula is a mountainous area located on the south coast of Livingston Island, South Shetlands, Antarctic (62°39′S, 60°21′W). About 90% of the island area is glaciated, with ice-free areas occurring at low altitude, generally in small but rugged peninsulas. This study focuses on ice-free areas in the northwestern part of Hurd Peninsula, in the vicinity of the Spanish Antarctic Station (SAS) Juan Carlos I (Figure 1). The altitude of the study sites ranges from 20 m asl near Juan Carlos I to 275 m asl on the summit of Reina Sofia Hill.

[18] The bedrock is a low-grade metamorphic turbidite sequence with alternating layers of quartzite and shales, with conglomerates and breccias in some areas (Miers Bluff Formation) [*Arche et al.*, 1992]. The whole succession dips 45° NW and is affected by open, primarily overturned folds [*Pallàs*, 1996]. The surficial lithology is very heterogeneous. Dolerite dykes and quartz veins are frequent [*Arche et al.*, 1992]. Differences in lithology induce different weathering styles and products. Quartzite shows high mechanical resistance, giving rise to convex landforms and a cover of large angular clasts. Shales are less resistant, giving rise to concave or flat topographies producing a sandy-silty matrix. Dykes show different characteristics depending on previous weathering of the rock.

[19] During isotope stage 2, Livingston Island was covered by an extensive ice cap. Only in the Holocene did deglaciation begin and some areas of the peninsulas became ice free (after 6.4 ka BP). Two glacier advances have been reported for the Holocene, the first between 720 and 330 BP and the other after 300 BP. This has been correlated to the Little Ice Age [*Pallàs*, 1996]. Glaciers are retreating steadily today.

3.2. Climate

[20] Climate at sea level is cold oceanic, with frequent summer rainfall and moderate annual temperature range. Data from different stations in King George Island show a mean annual air temperature of about −1.6°C near sea level and annual precipitation of about 500 mm (Department of Antarctic Biology, PAS [*Styszynska*, 2004]). Other air temperature data in the surroundings of Livingston Island show a mean air temperature range similar to Arctowski Station, with an average MAAT (excluding Faraday and Esperanza Station, which are too far from the South Shetland Islands, and Deception because of its limited data

Table 2b. Mean Annual Air Temperatures in the Northwestern Hurd Peninsula

	Spanish Station JCI (15 m asl), °C	Refugio Motos (165 m asl), °C	Reina Sofia Hill (275 m asl), °C
2003	−1.5	−2.9	−3.5
2004	−1.5	-	-
2005	−2.7	−2.4	−5.7

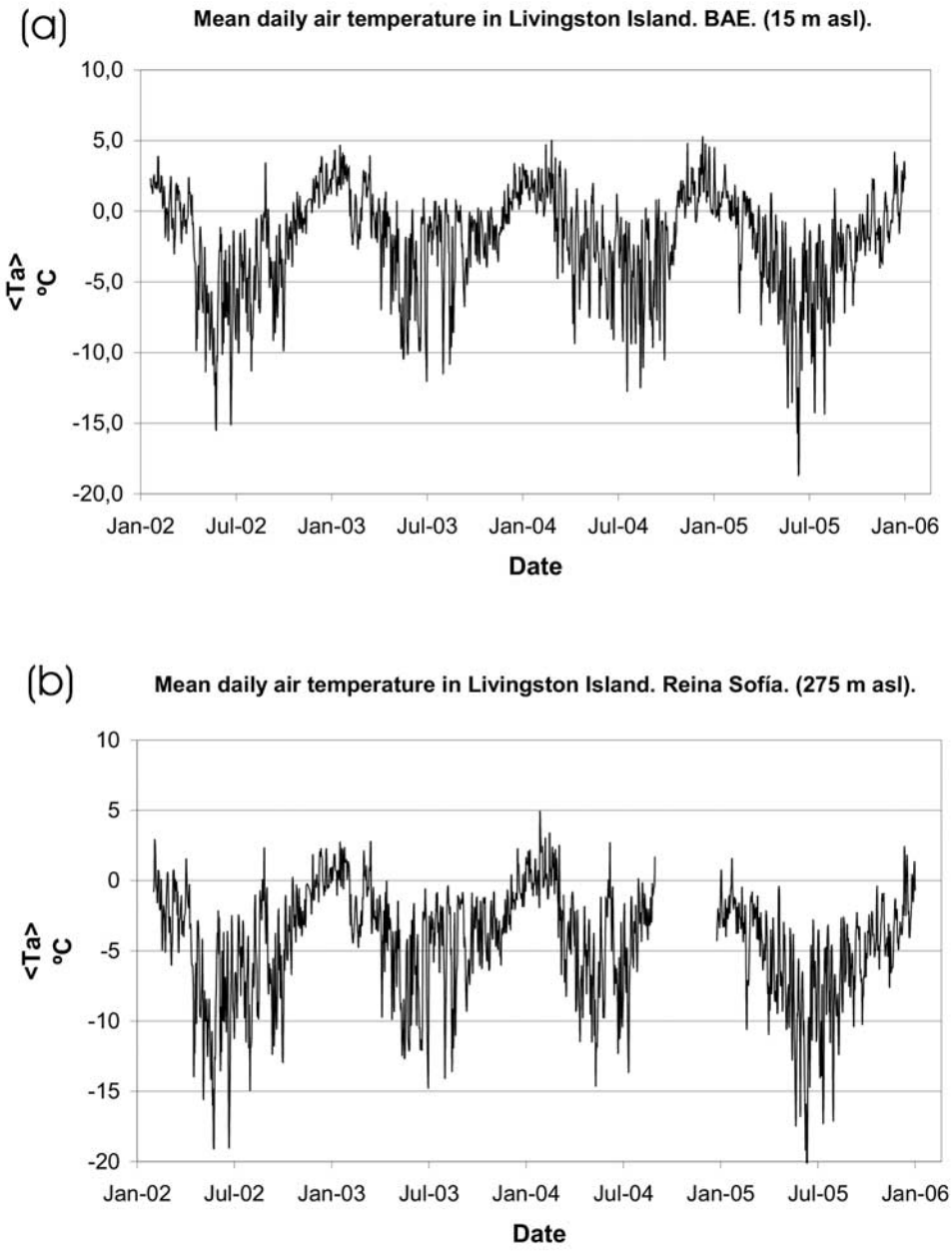

Figure 2. Mean daily air temperature at (a) Spanish Antarctic Station (15 m asl) and (b) Reina Sofia Hill (275 m asl).

period) of −1.9°C (Table 2a). Summer conditions are dominated by the continuous influence of polar frontal systems. Relative humidity is very high, with average values from 80 to 90% [*Simonov*, 1977; *Rakusa-Susczewski*, 1993].

[21] On the Hurd Peninsula, temperature records for the period 2003–2005 at 20 m asl show values comparable to those of the South Shetland Islands region (Table 2b). From April to November, average daily temperatures generally stay below 0°C, and from December to March temperatures are generally positive (Figure 2). The data describe the presence of a distinct seasonal frost cycle. At 275 m asl on Reina Sofia Hill the mean annual air temperature was about −4.2°C. This corresponds to a lapse rate of −0.8°C/100 m between the stations and the freezing season on Reina Sofia Hill is about one month longer than at sea level. According to *Serrano and López-Martínez* [2000], continuous permafrost occurs in the South Shetland Islands above the Holocene raised beaches (ca. 30 m asl).

3.3. Geomorphological Setting and Survey Sites

[22] Two geomorphological settings are of significance to present-day periglacial morphodynamics and permafrost distribution on the Hurd Peninsula: (1) an area veneered with till and containing well-developed moraine ridges in recently deglaciated valleys; and (2) an area with widespread angular debris mantling slopes and interfluves, in which deglaciation occurred earlier in the Holocene. The most widespread periglacial landforms are stone-banked lobes. Other periglacial features include patterned ground,

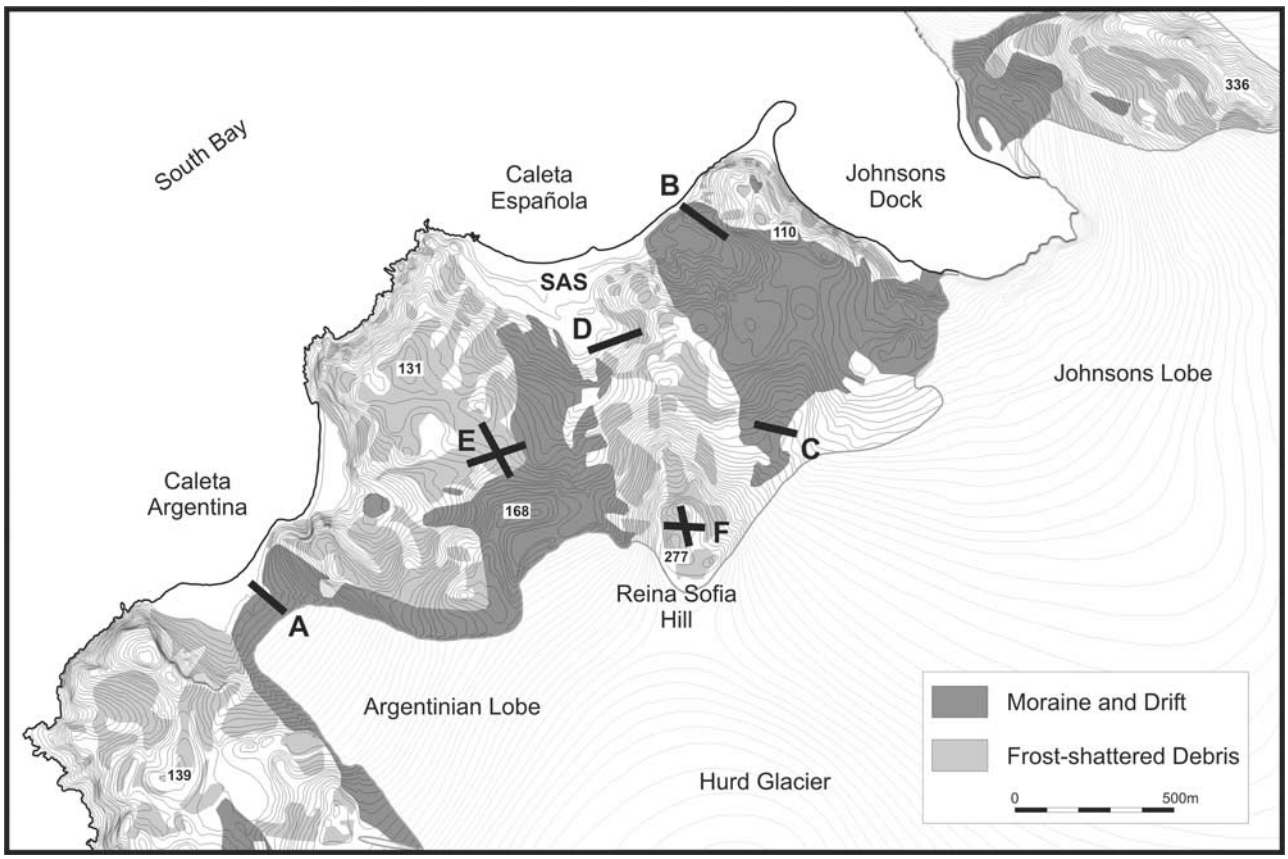

Figure 3. Location of survey sites in NW Hurd Peninsula: SAS, Spanish Antarctic Station; A, Caleta Argentina; B, Caleta Española; C, Refugio Motos; D, Incinerador; E, Collado Ramos; F, Reina Sofia.

especially in the higher, wind exposed interfluves (e.g., nonsorted circles on Reina Sofia Hill). Rock glaciers, of both the talus-derived (e.g., Johnsons Ridge) and the moraine-derived types (e.g., False Bay–Hurd) are present almost to sea level. Measurements were conducted on different moraine types, bedrock sites and unconsolidated sediments. For logistic reasons, no measurements on rock glaciers could be performed.

3.3.1. Caleta Argentina Moraine

[23] The Caleta Argentina site is located on the front moraine of the Argentinean lobe of Hurd Glacier (Figure 3). The moraine is about 15 m high and composed of nonsorted boulderly till. The moraine ridge is 50 m from the retreating glacier front and separated from it by a small outwash plain occupied by a meltwater stream that dissects the moraine. A shallow pond is in the northeast part of the outwash plain, showing a stable outflow of water, which is tapped from the glacier passing under the fluvioglacial sediment, which must be either frozen, or lying on top of glacier ice. Several active layer detachment slides occurred on the inner slopes of the moraine, and exposed a massive ice core in January 2000. Proximity to the glacier front, steepness of moraine slopes, widespread presence of fine material at the surface, and irregular surficial morphology indicate that the moraine is recent.

3.3.2. Caleta Española

[24] The Caleta Española site is on a moraine near the harbor of the SAS Juan Carlos I. The moraine system was deposited on the raised beach. Its lateral components run upvalley along the slopes. The measurement site is located in the lateral sector of the moraine, where it contacts the northwest slope of the valley. The site is at 30 m asl and the moraine rises 15–20 m above the valley floor. It is composed of boulderly diamicton with abundant sands and silts. *Pallàs* [1996] dated the moraine to between 330 and 720 yr BP. The glacier is located 700 m upstream. Along the deglaciated valley widespread till is present, showing numerous stone-banked solifluction lobes with frontal risers of 30–60 cm in height. The moraine surface shows signs of ongoing deformation, with fractures filled by collapsed sediment. The fractures, more than 10 m long and a few centimeters wide, run parallel to the slope, indicating movement toward the valley. A very steep inner moraine slope is in contact with the ephemeral stream on the valley floor, and therefore indicator of current deformation.

3.3.3. Refugio de Motos

[25] The Refugio de Motos site is on the northeast slope of Reina Sofia Hill at 145 m asl. The site was recently deglaciated and is 100 m from the glacier margin. Investigations were conducted on a roche moutonée covered by

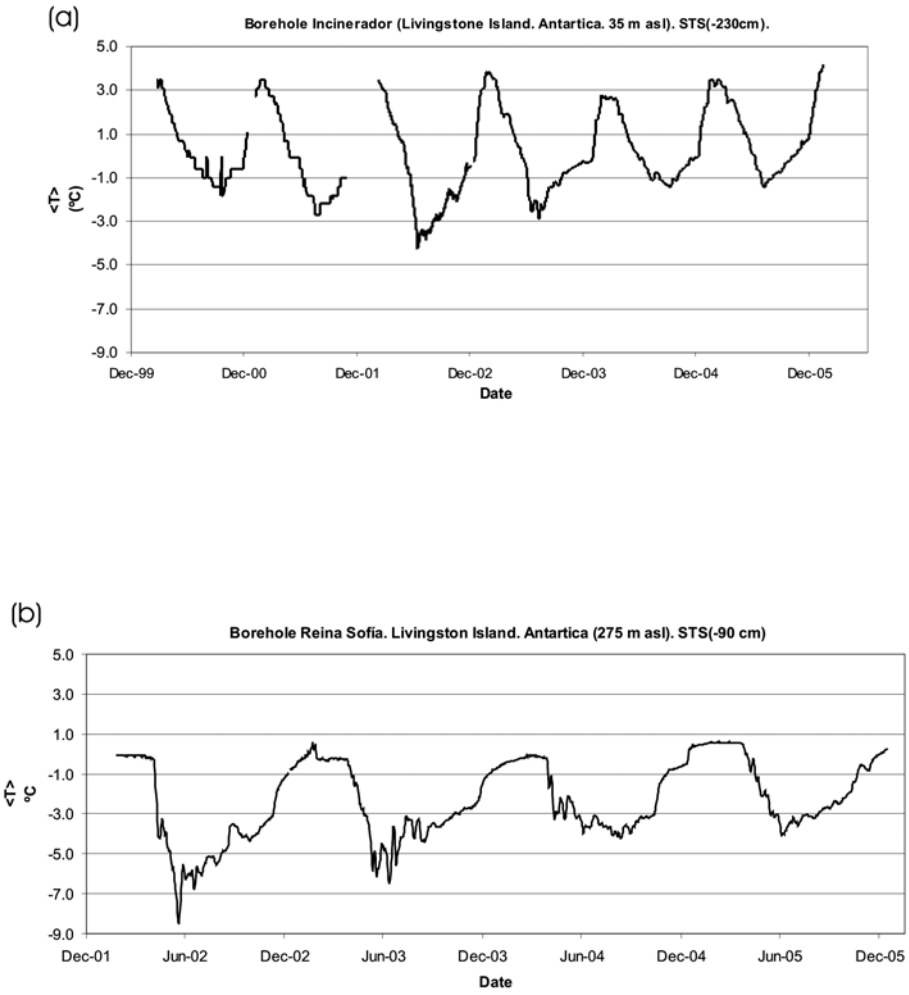

Figure 4. Mean daily ground temperatures at (a) 230 cm depth at Incinerador (site D) and (b) 90 cm depth at Reina Sofia (site F) for 2000–2005.

coarse boulderly till. Bedrock is composed of the Miers Bluff Formation, fine sandstone metasediments are dominant. The till sheet does not allow direct observation of the bedrock, however, and shales may be present in some places.

3.3.4. Incinerador

[26] The survey was conducted running parallel to a slope face near the Incinerador site where a shallow borehole is installed with temperature measurements down to 2.3 m depth since January 2000. The steep slope at this site is composed of quartzite and shale and incorporates a talus along which surveys were conducted. The talus is thin with bedrock outcrops. The talus is very heterogeneous, with some sectors dominated by angular quartzite boulders, and others showing coarse volcanogenic sands. This sandy material forms the matrix of the boulderly part of the talus. In the southwest part of the talus a stream originating from Hurd Glacier is present. Digging in the late 1990s in the lower part of the talus slopes has shown the presence of permafrost.

3.3.5. Collado Ramos

[27] The profiles are located in the saddle between the SAS valley and the Caleta Argentina site, at 115 m asl. The saddle is flat, 60 m wide, and its surface is mantled by an angular boulder diamicton with sandy matrix. Bedrock is the Miers Bluff Formation composed of alternating layers of quartzite and shale. At the surface, where the Miers Bluff Formation underlies the debris mantle, angular boulders occur. Where the bedrock is shaly, clasts are smaller and the matrix is finer and more abundant. Bedrock steeply dips toward the northwest. Dykes complicate the structure and interpretation of geophysical surveys. Alternating lichen-covered and lichen-free surfaces occur, and are likely to influence the ground energy budget. Lichens generally occur in the more wind-exposed sites and probably reflect a longer snow-free period.

3.3.6. Reina Sofia Hill

[28] Reina Sofia Hill is a small flat-topped mountain at 275 m asl overlooking the SAS valley. On the hill's south side Hurd Glacier covers the slope, but all other expositions are deglaciated and display steep slopes. Bedrock is com-

Table 3. Overview of Resistivities and *P* Wave Velocities Obtained at the Different Field Sites[a]

Location	Altitude, m asl	Specific Electrical Resistivity, ohm-m	*P* Wave Velocity, m/s	Active Layer Depth, m
Site A: Caleta Argentina ice core	30	7000–14000	-	2–3
Site A: Caleta Argentina unfrozen debris	30	1300–2000	-	2–3
Site B: Caleta Española ice core	30	25,000–40,000	2000–4000	2–3
Site B: Caleta Española unfrozen debris	30	1300–2000	300–1000	2–3
Site C: Refugio de motos debris	145	1300–2500	-	?
Site C: Refugio de motos quarzite/shale	145	2000–3000	-	?
Site D: Incinerador ash/fine sediments	35	1200–6000	500–1000	-
Site D: Incinerador quarzite/shale	35	1300–3500	2000–4000	-
Site E: Collado Ramos quarzite/shale	115	5000–8000	3500–5000	2
Site E: Collado Ramos weathered layer (AL)	115	2500–5000	500–1000	2
Site E: Collado Ramos weathered layer (PF)	115	10,000–20,000	?	2
Site F: Reina Sofia Hill quarzite/shale	275	7000–15000	2500–5500	0.8–1
Site F: Reina Sofia Hill weathered layer	275	1200–2500	500–1000	0.8–1

[a]AL is active layer; PF is permafrost.

posed of fine metamorphic sandstones at both ends of the profile and shales in the central area. On Reina Sofia a shallow borehole with temperature measurements down to 1.1 m depth has operated since January 2000. Pits dug in previous campaigns revealed a coarse weathering mantle decimeters to meters in thickness. Permafrost is present at 90–100 cm depth, as shown in the borehole data of Figure 4b.

4. Results

4.1. Borehole Temperatures

[29] The Incinerador borehole (dry bedrock) showed mean annual temperatures of 0.9°C in 2005 at 2.3 m depth. Minimum daily mean winter temperatures from 2000 to 2005 were −2°C to −3.5°C and summer daily mean maxima between 2.5°C and 4°C (Figure 4a). The temperature regime of the Reina Sofia borehole is different because of the higher altitude and latent heat effects. Mean annual temperature in 2005 was −1.4°C at 0.9 m depth and the permafrost table lies just below this level at ca. 1 m depth. Summer maxima during the period between 2002 and 2005 were between 0°C and 0.5°C and winter minima were between −4°C and −8.5°C (Figure 4b).

4.2. Geophysical Field Surveys

[30] An overview of typical values for different frozen and unfrozen material at the different field sites is given in Table 3. In the following the inversion results for both tomographic methods are presented and discussed for each field site.

4.2.1. Site A: Ice Cored Moraine, Caleta Argentina

[31] Figure 5 shows ERT results for the ice cored moraine in Caleta Argentina. The resistivity maximum of around 14,000 ohm-m denotes the ice core of the moraine, the region of highest ice content. Specific resistivities <2500–3000 ohm-m denote unfrozen morainic material within the active layer (2–3 m thick) and on the seaward side of the profile. These values are slightly less than the range of resistivity values found in previous VES surveys on Livingston Island for ice-rich permafrost, 10,000–150,000 ohm-m [*Serrano et al.*, 2004], and 35,000–77,000 ohm-m [*Bergamín et al.*, 1997], but are in good agreement with the generally reduced resistivity values in Arctic and Antarctic lowlands because of the enhanced salt content [*Guglielmin et al.*, 1997]. In comparison, they are about one magnitude less than corresponding resistivity values for ice cored moraines in the European Alps, where specific resistivities for ice cores may reach several hundreds of kohm-m and resistivities for unfrozen debris are about 10,000–50,000 ohm-m [e.g., *Hauck and Vonder Mühll*, 2003b].

4.2.2. Site B: Ice Cored Moraine, Caleta Española

[32] Similar to the moraine in Caleta Argentina, ERT results for unfrozen debris in the active layer of the ice

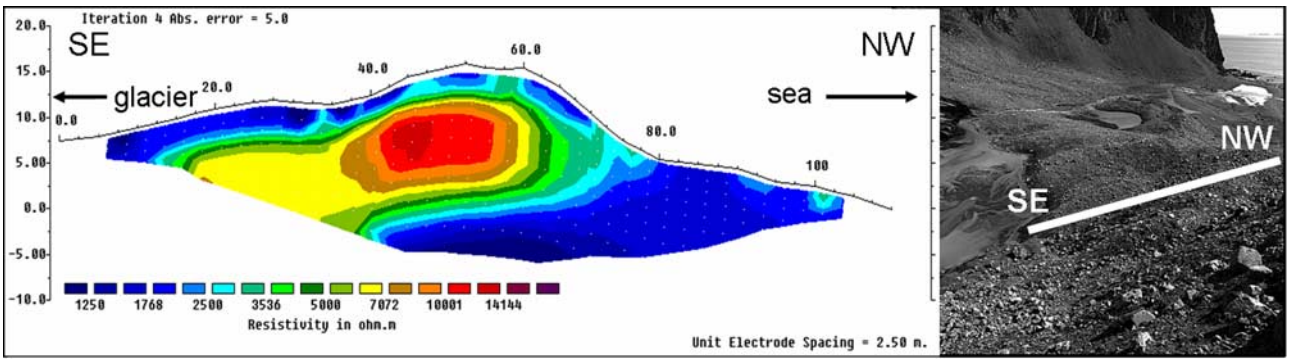

Figure 5. ERT survey results and photo of ice cored moraine at Caleta Argentina (site A). For location of profile, see Figure 3.

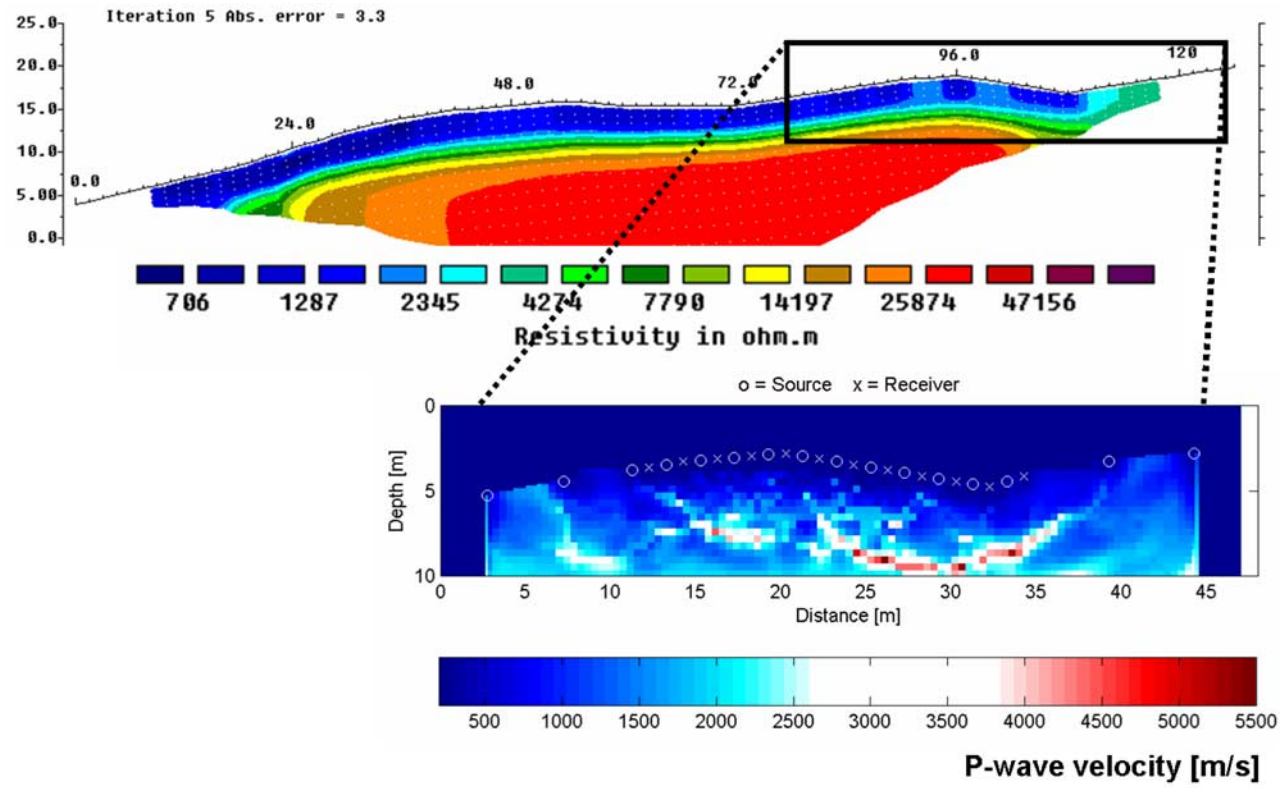

Figure 6. ERT survey results and seismic refraction results of the moraine near the Spanish Antarctic Station (Caleta Española, site B). Black rectangle marks location of seismic profile. For location of profile, see Figure 3.

cored moraine in Caleta Española show specific resistivities less than 2000 ohm-m, indicating the presence of the same kind of morainic material at both field sites (Figure 6). Active layer depths at both sites are in very good agreement (2–3 m). Specific resistivities of the Caleta Española ice core are higher (25,000–40,000 ohm-m), which could indicate a larger ice content or smaller unfrozen water content than at Caleta Argentina. Forward model studies with synthetic data sets showed that, in addition to the unfrozen water/ice content, the geometry of the ERT survey may have had a significant influence on the absolute values of highly resistive and geometrically constrained anomalies. At a field site similar to site A, *Hauck and Vonder Mühll* [2003b] showed that cross sections over ice cored moraines may artificially reduce the maximum specific resistivities obtained in the inversion results, whereas longitudinal sections (as with site B) are more accurate concerning the maximum specific resistivities. Longitudinal sections are, however, less suitable to detect the lower boundary of the ice core. Confirming this, the cross section at site A clearly detects the lower boundary of the ice core (at 15 m depth), whereas no lower boundary can be seen in the longitudinal profile at site B. On the contrary, the maximum specific resistivities of the latter (40,000 ohm-m) may be nearer to reality than the 14,000 ohm-m obtained at site A.

[33] The corresponding refraction seismic profile (Figure 6) shows low *P* wave velocities (<1000 m/s) in the uppermost 2–3 m, indicating the unfrozen active layer, and velocities between 2000–4000 m/s for the ice core, pointing to a probable high ice content.

4.2.3. Site C: Refugio de Motos

[34] Figure 7 shows ERT results for the survey line at Refugio de Motos. The relatively uniform specific resistivity values around 2000–3000 ohm-m indicate the quartzite. Values below 2000 ohm-m indicate the debris cover, as seen in Figures 5 and 6. At the western margin of the large-scale profile (Figure 7a), a high-resistive anomaly at about 2 m depth can be identified in this otherwise homogeneous resistivity model. This anomaly coincides with comparatively low-resistivity values at the surface, where fine-grained debris was found. Keeping in mind that the inversion model has especially low accuracy at the model margins, this anomaly could be interpreted as indicating the presence of permafrost with higher ice content than within the bedrock elsewhere in the profile. If this is true, the active layer depth at this site could be identified as around 2 m. However, the generally low-resistivity values within most of the profile, compared to the maximum values at sites A and B, do not give any clear indication of the presence of ice. High ice contents can be excluded.

4.2.4. Site D: Incinerador

[35] Figure 8 shows results for the survey line at Incinerador, where measurements in a shallow borehole recorded positive ground temperatures in summer, down to at least 2.3 m depth (Figure 4a). Resistivity values below this depth are uniformly distributed over the range 1300–2500 ohm-m, except for the eastern part of the profile, where slightly larger values are found. Within the uppermost 2 m, *P* wave velocities below 1000 m/s and high-resistive anomalies up to 6000 ohm-m indicate the presence of dry, loosely sorted

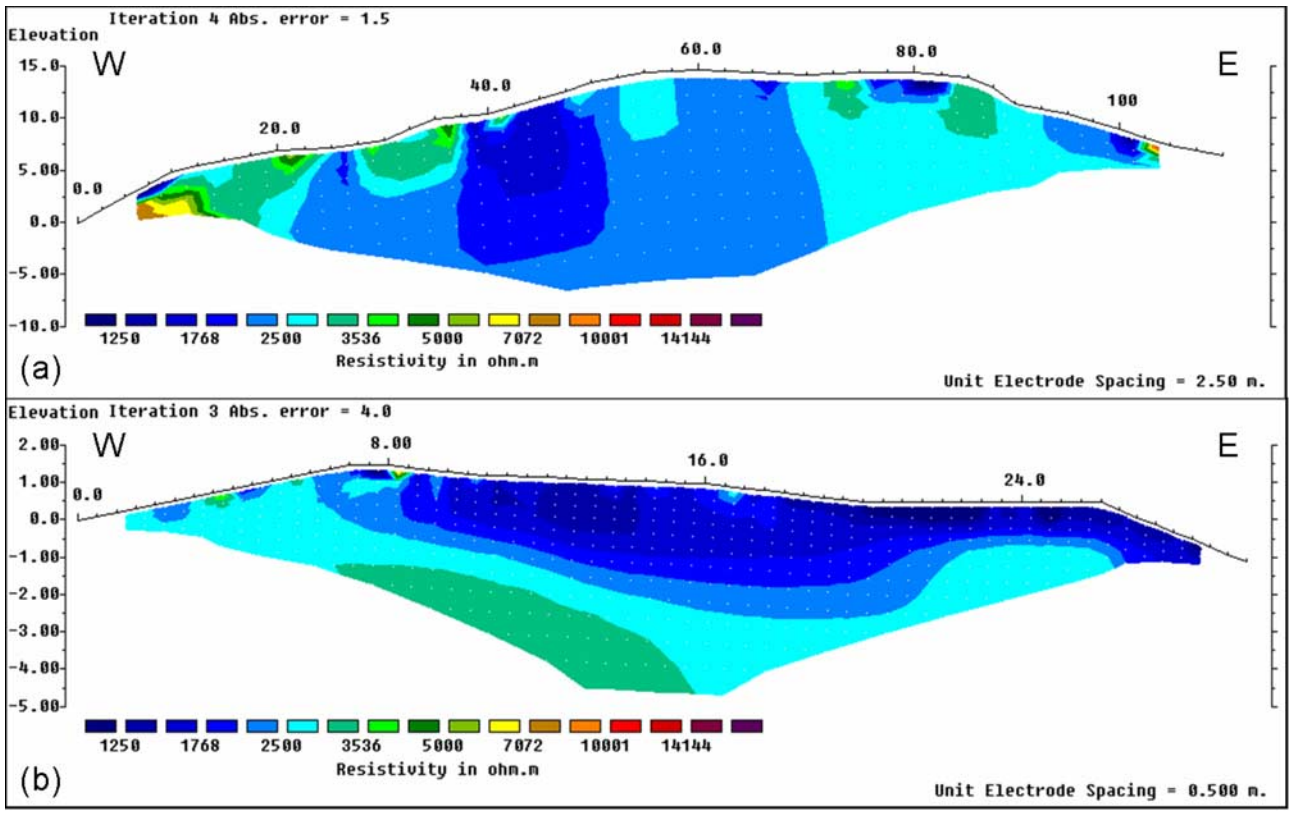

Figure 7. ERT survey results at Refugio de Motos (site C): (a) large-scale and (b) small-scale survey. For location of profile, see Figure 3.

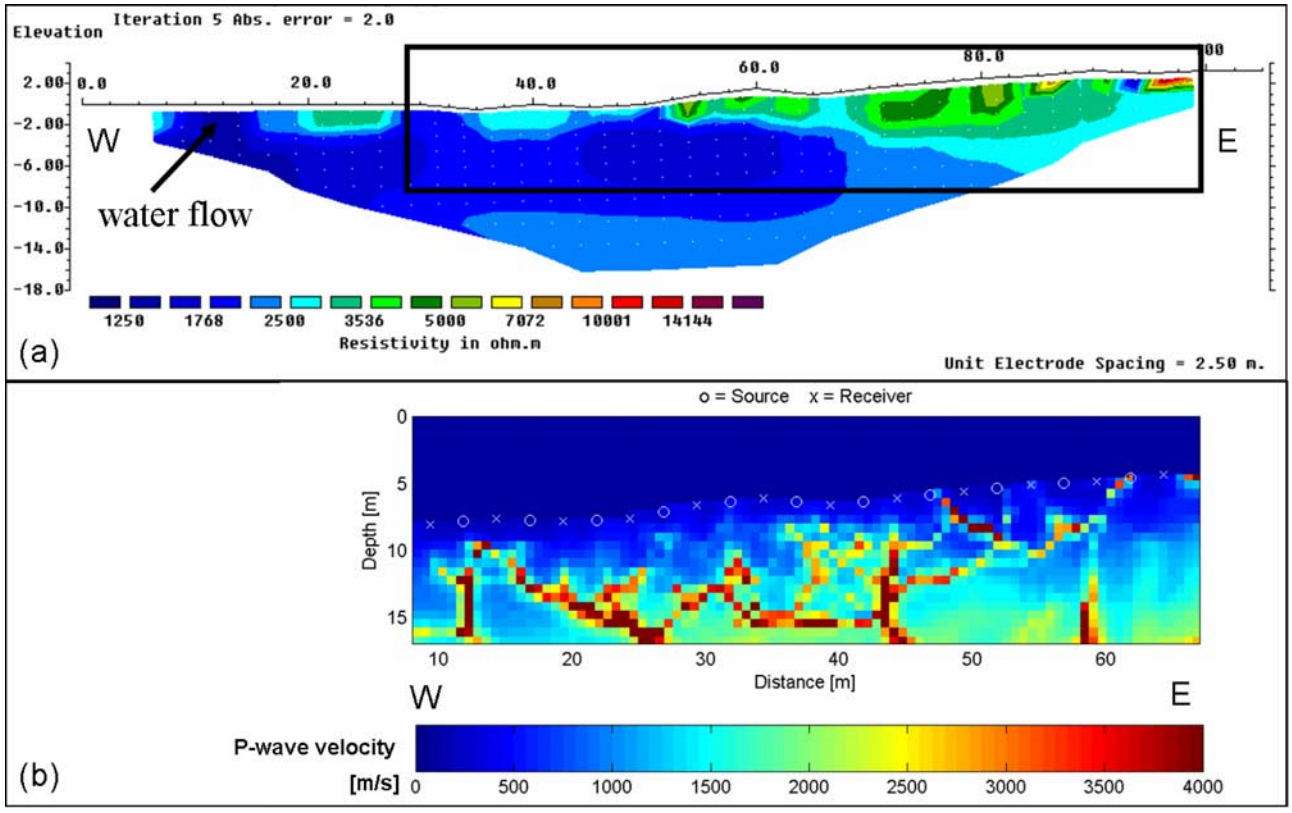

Figure 8. (a) ERT survey results and (b) seismic refraction results at Incinerador site (site D). Black rectangle marks location of seismic profile. For location of profile, see Figure 3.

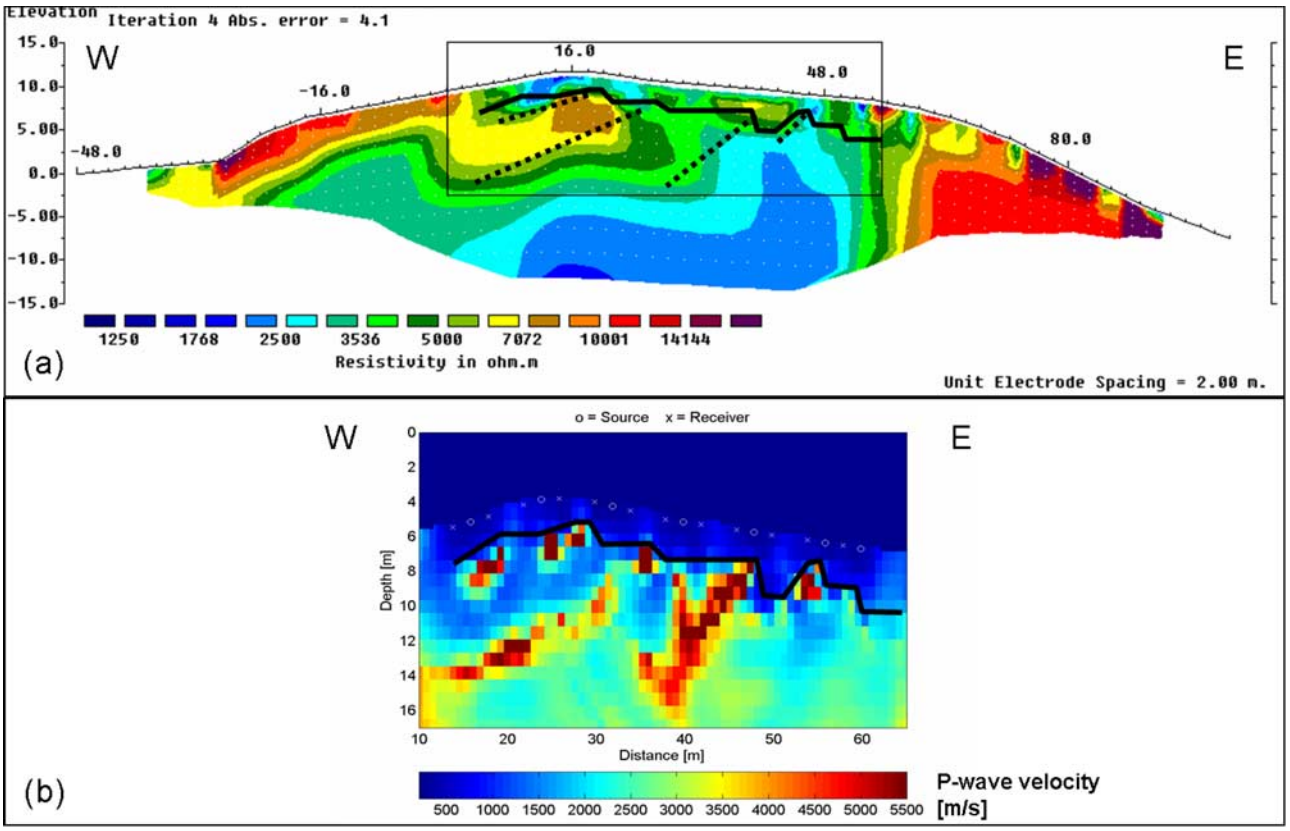

Figure 9. (a) ERT survey results and (b) seismic refraction results of E–W profile at Collado Ramos (site E). Rectangle in Figure 9a marks location of seismic profile. Dashed and solid lines delineate high-velocity structures in Figure 9b. For location of profile, see Figure 3.

material with comparatively large air content [e.g., *Hauck and Vonder Mühll*, 2003b]. Below this surficial layer *P* wave velocities between 2000–4000 m/s are present, indicating either bedrock at a depth of 5–10 m or frozen material. The latter is not very probable because ground temperatures at 2.3 m depth are comparatively warm (Figure 4a). The corresponding low-resistivity values of less than 3500 ohm-m indicate an absence of high ice contents. However, an enhanced salt content and/or a high unfrozen water content could mask the presence of significant ice contents [*Guglielmin et al.*, 1997]. *Bergamín et al.* [1997] used geophysical soundings and geomorphological interpretation to determine the position of a bedrock layer at a depth of around 30 m near this site. The high *P* wave velocities could therefore indicate a permafrost layer at around 5 m depth, although it would have to consist of very warm permafrost with high salt/unfrozen water content to explain the observed low resistivities and comparatively high temperatures.

4.2.5. Site E: Collado Ramos

[36] Figure 9 shows ERT and seismic results for the E–W profile at Collado Ramos at 115 m asl. Again, low *P* wave velocities of less than 1000 m/s in the uppermost 2 m indicate unfrozen weathered material (solid line in Figure 9). Corresponding specific resistivity values (black rectangle) are slightly higher (2500–5000 ohm-m) compared to sites A–D. However, this pattern is altered outside the black rectangle, which marks the area covered by the seismic profile. Here, specific resistivities greater 10,000 ohm-m are found at the surface reaching 5 m depth in the west and more than 10 m in the east. Extremely high-resistive anomalies greater 20,000 ohm-m are found at the surface, and are related to perennial snow patches visible during the survey in February 2006. Unfortunately, seismic velocities are not available in this part of the profile, although the combination of snow patches at the surface and high resistivities at depth strongly suggest the presence of permafrost beneath both flanks of Collado Ramos.

[37] *P* wave velocities of 3500–5000 m/s are found at greater depth below the center of the profile. The dipping structure of these high-velocity zones (dashed lines in Figure 9) indicates a connection with the dipping bedrock structures found at the surface. The high-velocity zones are in good agreement with resistive structures (>5000 ohm-m) found in the ERT results, and could indicate frozen bedrock with ice occurrences within the (dipping) cracks and fissures. On the other hand, similar velocity and resistivity values could be observed in unfrozen bedrock, so an interpretation of permafrost is not conclusive from the geophysical results alone. However, on the basis of a combination of all results (Figure 12 and section 5) we favor an interpretation that permafrost could be present at this altitude with thickness of 5 m in the west, 10 m in the center and more than 10 m in the east.

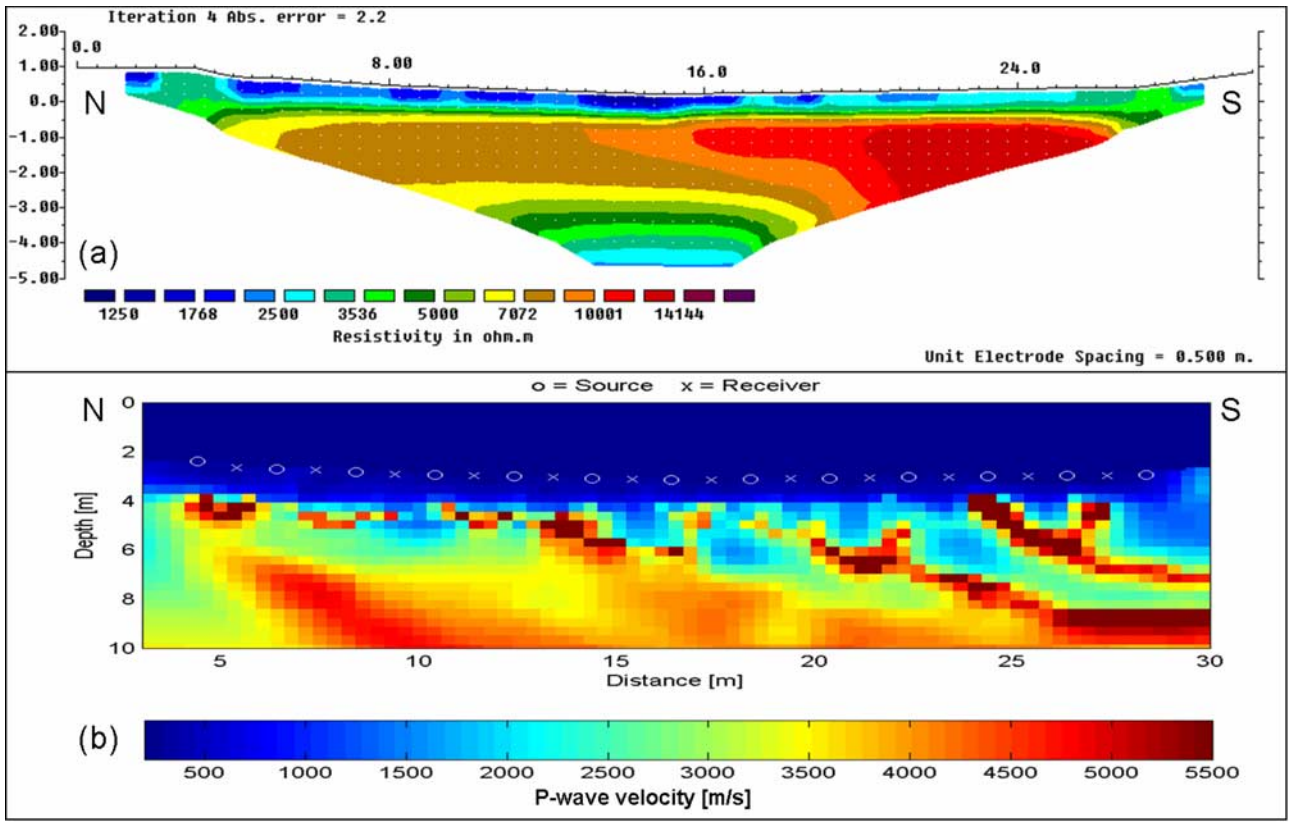

Figure 10. (a) ERT survey results and (b) seismic refraction results of N–S profile at Reina Sofia Hill (site F). For location of profile, see Figure 3.

4.2.6. Site F: Reina Sofia Hill

[38] Figure 10 shows results for the highest field site, Pico Reina Sofia (275 m asl). Both profiles show a rather uniform subsurface, with low-resistivity values (1250–2500 ohm-m) and low *P* wave velocities (500–1000 m/s) in the uppermost 0.8–1 m and high resistivities (7000–15,000 ohm-m) and high velocities (2500–5500 m/s) below. From the temperature measurements at Reina Sofia (20 m east of the survey line center) active layer depth is around 0.9 m (Figure 4b). This value coincides with the depth of the boundary between the low-resistivity/velocity region above and the high-resistivity/velocity layer below. The values of the unfrozen top layer are in good agreement with those obtained at the other sites, whereas the values of the lower frozen layer are significantly higher than the corresponding values observed at other bedrock sites, Refugio de Motos, Incinerador and Collado Ramos (C, D, and E). The presence of permafrost is confirmed through the borehole data at these sites, and the increased values can be attributed to higher ice content and lower unfrozen water content within the cracks and fissures of the bedrock.

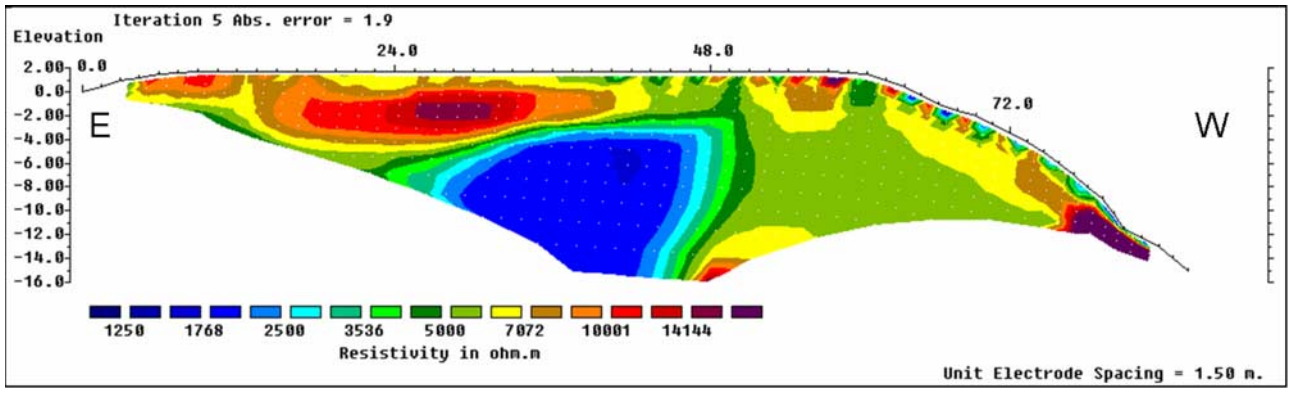

Figure 11. E–W oriented ERT survey results with increased depth penetration at Reina Sofia Hill (site F). For location of profile, see Figure 3.

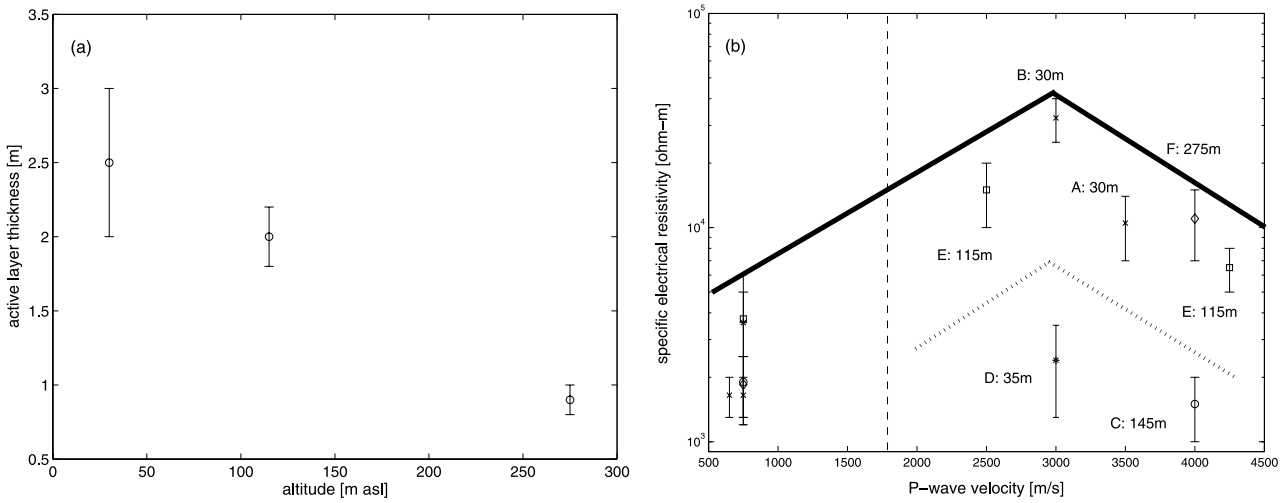

Figure 12. Comparison of (a) active layer thickness and altitude and (b) observed specific electrical resitivities and seismic *P* wave velocities at different field sites. Solid line in Figure 12b denotes upper limit of observed values. Vertical dashed line marks the boundary between the permafrost-free sites to the left and the possible permafrost sites to the right, inferred from *P* wave velocities. Dashed line denotes lower limit of possible permafrost sites, inferred from resistivities and *P* wave velocities. Letters and altitudes for each site are given for each data pair.

[39] Problems of interpretation arise from the decreasing resistivities observed below 4–5 m depth (Figure 10a). Figure 11 presents ERT survey results with increased depth penetration, showing consistent resistivity values in the uppermost 5 m and a low-resistivity zone at greater depth. This result can be interpreted as shallow permafrost or the presence of low-resistive bedrock. The climate data (MAAT = −4.2°C) and the borehole results indicate that permafrost thickness of only 5 m is highly unlikely. Moreover, the presence of adjacent high-resistive zones at greater depth points to the presence of bedrock material with different resistivity, such as the shale layer observed at the surface, or possibly different total and unfrozen water contents.

5. Discussion

[40] The geophysical tomograms emphasize the strong relation between reliability of interpretation and permafrost characteristics, especially ice content. Morphologic features with high ice content are detected clearly, but difficulties arise when different lithologies with small ice contents are compared. Use of complementary methods greatly improves interpretation, especially if the physical principles underlying the methods are different.

[41] Geoelectric methods are especially sensitive to changes in unfrozen water content, because electrical current is transported through ionic conduction within the liquid phase. Consequently, the presence of ice is inferred mainly from the absence of ionic conduction, that is, if the specific resistivity is high. As this is the case for both air-filled and ice-filled pore spaces and fissures, geoelectric methods are not generally suitable for distinguishing between dry unfrozen and frozen ground conditions.

[42] In contrast, seismic wave energy is transported through the solid phase, which consists either of ice or a bedrock matrix. In unconsolidated material with comparatively large air content (debris or morainic material), the presence of ice is easily detected, even for very warm permafrost conditions with large unfrozen water content. In bedrock, the increase in *P* wave velocity resulting from the presence of ice in cracks and fissures is small, but can be detected in homogeneous bedrock [e.g., *McGinnis et al.*, 1973]. For different bedrock types within the same area, difficulties arise, as the change in *P* wave velocity attributed to varying lithology is usually larger than that resulting from variations in ground temperature or ice content.

[43] In a morphologically complex environment such as Livingston Island, permafrost distribution is unlikely to be determined by simple altitude-aspect relations. Owing to the short summer season where snow-free conditions prevail only for 2–3 months, the timing and spatial variability of the snow cover is of utmost importance for the ground thermal regime. Unfortunately, snow cover data are largely unavailable. To overcome the lack of data, snow poles with temperature sensors at different heights were installed in 2006 to better combine ground thermal, geophysical and climatic data at the different survey sites. Until results from this instrumentation are available, permafrost conditions will have to be inferred from the temperature and geophysical data sets presented above.

[44] Figure 12a shows the dependence of active layer depth on altitude, as inferred from the geophysical data sets. Even though the amount of data is too sparse to determine a statistically significant relation, an indication was found, with active layer thickness of 2–3 m near sea level and less than 1 m at 275 m asl on Reina Sofia Hill. The dependence of specific electrical resistivity values and *P* wave velocity on altitude is less obvious because of the strong influence of material composition.

[45] Figure 12b shows mean specific electrical resistivities and *P* wave velocities for the different survey sites. Because the range of *P* wave velocities obtained within the tomograms (see Table 3) is very large, they were not

included for clarity. For each survey site two data pairs, corresponding to values found in the surficial (or active) layer and below, were included. The data pairs in the lower left corner of Figure 12b were all taken from the surficial layer and denote the unfrozen conditions in the active layer at all survey sites. This is mainly confirmed by the low *P* wave velocities in unfrozen and unconsolidated material.

[46] The distribution of data pairs from deeper levels is scattered and dependent on material type and altitude. A typical feature in Figure 12b is the ''roof-type'' distribution, where maximum resistivity values are found at intermediate *P* wave velocities around 3000 m/s and declining resistivities on either side. This is because maximum resistivities occur in ice-rich permafrost (e.g., within rock glaciers, debris cones and the ice cored moraines in Caleta Argentina and Española) consisting of supersaturated ice with typical *P* wave velocities between 3000–3750 m/s. For decreasing ice contents in unconsolidated material, both resistivities and *P* wave velocities decrease (left side of the ''roof'', e.g., area below the perennial snow patches at Collado Ramos (site E)), whereas for decreasing ice contents in bedrock *P* wave velocity increases with decreasing resistivity (such as the bedrock on Reina Sofia Hill (site F) and Collado Ramos (site E)). Low-porosity bedrock with low ice content typically shows high *P* wave velocities due to the better propagation of the seismic wave energy. Combining these considerations, a subregion in the resistivity/velocity space is identified in Figure 12b, which may serve as an indicator for the presence of permafrost on Livingston Island (shown by the hatched area).

[47] No definite conclusion about permafrost thickness can be drawn from the geophysical data sets. Near sea level, conditions are variable and depend strongly on morphology and snow cover distribution. Although no clear indication of the presence of permafrost was found at the Incinerador site at 35 m asl, where ground temperatures are still largely positive at 2.3 m depth, ice cores of probable glacial origin were found within two moraines close to the sea. The thickness of the 10 m ice core was determined with ERT, but only when using a survey geometry perpendicular to the core axis. At higher altitudes, ice-rich permafrost was found only in the weathered surface layer at depths between 2–5 m (Collado Ramos and Reina Sofia). However, permafrost thickness underlying bedrock could not be determined because of the heterogeneous lithology of strongly dipping quartzite and shale layers.

6. Conclusion

[48] Permafrost distribution on Livingston Island was investigated using multiple geophysical data sets obtained during the austral summer field work campaign in 2006. Key results from this preliminary study include:

[49] 1. Permafrost is widespread on Livingston Island. It is evident in typical periglacial features like ice cored moraines and rock glaciers with comparatively high ice content, and in frozen bedrock with little ice content within cracks and fissures.

[50] 2. Active layer thickness depends strongly on altitude. Values range from 2–3 m near sea level to 0.8–1 m at 275 m asl.

[51] 3. Specific electrical resistivity values in frozen unconsolidated material show a typical range of 10,000–40,000 ohm-m, whereas values in frozen bedrock (quartzite and shale) range between 1500 and 10,000 ohm-m, depending on unfrozen water/salt content and bedrock type.

[52] 4. *P* wave velocities below 1500 m/s confirm the absence of permafrost, whereas specific electrical resistivities above 7000 ohm-m are a strong indication of the presence of permafrost in this region.

[53] 5. Caution must be exercised when comparing maximum specific electrical resistivity values obtained with different geometries in topographically structured terrain. Profiles perpendicular to the axis of a high-resistive anomaly lead to underestimation of maximum specific resistivities. In contrast, the lower boundary of a high-resistive anomaly is better delineated for surveys with perpendicular orientation. Both effects are strongest for the Wenner electrode array.

[54] 6. Combining *P* wave velocities and specific electrical resistivities within a joint diagram a typical ''roof-type'' distribution is found with maximum resistivities coinciding with *P* wave velocities around 3000 m/s and decreasing resistivities for both increasing and decreasing velocities.

[55] 7. We were unable to determine permafrost thickness from the geophysical data sets because of the heterogeneous lithology and strongly dipping quartzite and shale layers. Temporal and spatial variations in snow cover thickness may have contributed to these difficulties.

[56] The results presented in this paper highlight the feasibility of using noninvasive geophysical techniques for characterizing frozen ground conditions in permafrost environments. Surveys can be performed both to delineate suitable locations for planned boreholes, as well as to analyze large-scale ground conditions after the drilling to determine the spatial significance of borehole results. The results of this study are significant for choosing the planned borehole locations and serve as a baseline for future monitoring efforts on Livingston Island.

[57] **Acknowledgments.** This study was conducted as part of the PERMAMODEL project within the Spanish Antarctic Program CICyT (CGL2004-20896-E/ANT). We thank participants of the campaign at the Spanish Antarctic Station Juan Carlos I and the research vessels BIO *Las Palmas* and BIO *Hesperides* for their kind support. Constructive and very useful comments of F. Nelson and an anonymous reviewer are gratefully acknowledged.

References

Arche, A., J. López-Martínez, and E. Martínez de Pisón (1992), Sedimentology of the Miers Bluff formation, Livingston Island, South Shetland Islands, in *Recent Progress in Antarctic Earth Science*, edited by Y. Yoshida et al., pp. 357–362, Terra Sci., Tokyo.

Bergamín, J. F., J. J. Durán, J. M. González-Casado, and J. López-Martínez (1997), Morfología y estructura del basamento precuaternario de la Caleta Española, Peninsula Hurd, Isla Livingston, *Bol. Real Soc. Esp. Hist. Nat.*, *93*(1–4), 189–196.

Bockheim, J. G., and K. J. Hall (2002), Permafrost, active-layer dynamics and periglacial environments of continental Antarctica, *S. Afr. J. Sci.*, *98*, 82–90.

Daily, W., A. Ramirez, A. Binley, and D. LaBrecque (2004), Electrical resistance tomography, *Leading Edge*, *23*(5), 438–442.

Fournier, H. G., E. M. Buk, and A. E. Corte (1990), Three permafrost conditions indicated by geophysical soundings in tertiary sediments at Seymour Island, Antarctic Peninsula, *Cold Reg. Sci. Technol.*, *17*, 301–307.

Guglielmin, M., A. Biasini, and C. Smiraglia (1997), Buried ice landforms in the northern foothills (Northern Victoria Land, Antarctica). Some results from electrical soundings, *Geogr. Ann., Ser. A*, *79*(1–2), 17–24.

Hall, K. (2002), Review of present and quaternary periglacial processes and landforms of the maritime and sub-Antarctic region, *S. Afr. J. Sci.*, *98*, 71–81.

Hauck, C., and D. Vonder Mühll (2003a), Evaluation of geophysical techniques for application in mountain permafrost studies, *Z. Geomorphol. Suppl.*, *132*, 159–188.

Hauck, C., and D. Vonder Mühll (2003b), Inversion and interpretation of 2-dimensional geoelectrical measurements for detecting permafrost in mountainous regions, *Permafrost Periglacial Processes*, *14*, 305–318.

Hauck, C., K. Isaksen, D. Vonder Mühll, and J. L. Sollid (2004), Geophysical surveys designed to delineate the altitudinal limit of mountain permafrost: An example from Jotunheimen, Norway, *Permafrost Periglacial Processes*, *15*, 191–205.

Hoekstra, P., P. V. Sellmann, and A. Delaney (1975), Ground and airborne resistivity surveys of permafrost near Fairbanks, Alaska, *Geophysics*, *40*, 641–656.

Hubbard, B., and N. Glasser (2005), *Field Techniques in Glaciology and Glacial Geomorphology*, John Wiley, Chichester, U. K.

Intergovernmental Panel on Climate Change (2001), *Climate Change 2001: The Scientific Basis. Contribution of Working Group I to the Third Assessment Report of the Intergovernmental Panel on Climate Change (IPCC)*, edited by J. T. Houghton et al., Cambridge Univ. Press, New York.

King, M. S., R. W. Zimmerman, and R. F. Corwin (1988), Seismic and electrical properties of unconsolidated permafrost, *Geophys. Prospect.*, *36*, 349–364.

Kneisel, C., C. Hauck, and D. Vonder Mühll (2000), Permafrost below the timberline confirmed and characterized by geoelectrical resistivity measurements, Bever Valley, eastern Swiss Alps, *Permafrost Periglacial Processes*, *11*, 295–304.

Lanz, E., H. R. Maurer, and A. G. Green (1998), Refraction tomography over a buried waste disposal site, *Geophysics*, *63*, 1414–1433.

Loke, M. H., and R. D. Barker (1995), Least-squares deconvolution of apparent resistivity, *Geophysics*, *60*, 1682–1690.

McGinnis, L. D., K. Nakao, and C. C. Clark (1973), Geophysical identification of frozen and unfrozen ground, Antarctica, in *Proceedings, Second International Conference on Permafrost*, vol. 1287, pp. 136–146, Natl. Acad. of Sci., Ottawa.

Musil, M., H. R. Maurer, A. G. Green, H. Horstmeyer, F. Nitsche, D. Vonder Mühll, and S. Springman (2002), Shallow seismic surveying of an Alpine rock glacier, *Geophysics*, *67*, 1701–1710.

Pallàs, R. (1996), Geologia de l'Illa de Livingston (Shetland del Sud, Antàrtida). Del Mesozoic al present, Ph.D. thesis, Univ. Barcelona, Barcelona, Spain.

Rakusa-Susczewski, S. (1993), The maritime Antarctic coastal ecosystem of Admiralty Bay, Dep. of Antarct. Biol., Pol. Acad. of Sci., Warsaw.

Ramos, M., and G. Vieira (2003), Active layer and permafrost monitoring in Livingston Island, Antarctic. First results from 2000 and 2001, in *Permafrost*, *Proceedings of the Eight International Conference on Permafrost, 21–25 July 2003, Zürich*, edited by M. Phillips et al., pp. 929–933, A. A Balkema, Lisse, Netherlands.

Ramos, M., G. Vieira, F. Crespo. and L. Bretón (2002), Seguimiento de la evolución temporal del gradiente térmico de capa activa en las proximidades de la BAE Juan Carlos I (Antártida), in *Periglaciarismo en Montaña y Altas Latitudes*, edited by E. Serrano and A. García, pp. 257–276, Univ. de Valladolid, Valladolid, Spain.

Scott, W., P. Sellmann, and J. Hunter (1990), Geophysics in the study of permafrost, in *Geotechnical and Environmental Geophysics*, edited by S. Ward, pp. 355–384, Soc. of Explor. Geophys., Tulsa, Okla.

Serrano, E. (2003), Paisaje natural y pisos geoecologicos en las áreas libres de hielo de la Antártida Marítima (Islas Shetland del Sur), *Bol. A. G. E.*, *35*, 5–32.

Serrano, E., and J. López-Martínez (2000), Rock glaciers in the South Shetland Islands, Western Antarctica, *Geomorphology*, *35*, 145–162.

Serrano, E., J. Giner, P. Gumiel, and J. López-Martínez (2004), El glaciar rocoso de Hurd: Estructura e inserción en el sistema de transferencia de derrubios Antárctico marítimo (Islas Shetland del Sur, Antártida), *Rev. Cuat. Geomorfol.*, *18*(1–2), 13–24.

Simonov, I. M. (1977), Physical geographic description of Fildes Peninsula (South Shetland Islands), *Polar Geogr.*, *1*, 223–242.

Styszynska, A. (2004), The origin of coreless winters in the South Shetlands area (Antarctica), *Pol. Polar Res.*, *25*, 45–66.

Timur, A. (1968), Velocity of compressional waves in porous media at permafrost temperatures, *Geophysics*, *33*, 584–595.

Vieira, G., and M. Ramos (2003), Geographic factors and geocryological activity in Livingston Island, Antarctic. Preliminary results, in *Permafrost*, *Proceedings of the Eight International Conference on Permafrost, 21–25 July 2003, Zürich*, edited by M. Phillips et al., pp. 1183–1188, A. A. Balkema, Lisse, Netherlands.

Zimmerman, R. W., and M. S. King (1986), The effect of freezing on seismic velocities in unconsolidated permafrost, *Geophysics*, *51*, 1285–1290.

J. Blanco and M. Ramos, Department of Physics, University of Alcalá, E-28871 Alcalá de Henares, Spain.

S. Gruber, Glaciology and Geomorphodynamics Group, Department of Geography, University of Zurich, Winterthurerstr. 190, CH-8057 Zurich, Switzerland.

C. Hauck, Institute for Meteorology and Climate Research, Forschungszentrum Karlsruhe, University of Karlsruhe, Postfach 3640, D-76021 Karlsruhe, Germany. (hauck@imk.fzk.de)

G. Vieira, Centre for Geographical Studies, Faculdade de Letras, University of Lisbon, Alameda da Universidade, P-1600-214 Lisboa, Portugal.